Damage and ablation thresholds of fused-silica in femtosecond regime

B. Chimier,[1,*] O. Utéza,[1] N. Sanner,[1] M. Sentis,[1] T. Itina,[2] P. Lassonde,[3] F. Légaré,[3] F. Vidal,[3] and J. C. Kieffer[3]

[1]*Laboratoire LP3, UMR 6182 CNRS – Université de la Méditerranée, C. 917, 163, Av. de Luminy, 13288 Marseille cedex 9, France*

[2]*Laboratoire Hubert Curien – LaHC, UMR 5516 CNRS – Université Jean Monnet, Bât. F, 18, rue Professeur B. Lauras, 42000 Saint-Etienne, France*

[3]*INRS, Energie, Matériaux et Télécommunications, 1650 bld Lionel Boulet, Varennes (Québec), Canada, J3X 1S2*

(Received 19 November 2010; revised manuscript received 20 July 2011; published 19 September 2011)

We present an experimental and numerical study of the damage and ablation thresholds at the surface of a dielectric material, e.g., fused silica, using short pulses ranging from 7 to 300 fs. The relevant numerical criteria of damage and ablation thresholds are proposed consistently with experimental observations of the laser irradiated zone. These criteria are based on lattice thermal melting and electronic cohesion temperature, respectively. The importance of the three major absorption channels (multi-photon absorption, tunnel effect, and impact ionization) is investigated as a function of pulse duration (7–300 fs). Although the relative importance of the impact ionization process increases with the pulse duration, our results show that it plays a role even at short pulse duration (<50 fs). For few optical cycle pulses (7 fs), it is also shown that both damage and ablation fluence thresholds tend to coincide due to the sharp increase of the free electron density. This electron-driven ablation regime is of primary interest for thermal-free laser-matter interaction and therefore for the development of high quality micromachining processes.

DOI: 10.1103/PhysRevB.84.094104 PACS number(s): 79.20.Ds, 52.50.Jm, 42.65.Re

I. INTRODUCTION

Interaction of femtosecond laser pulses with dielectric materials is of sound significance both for fundamental knowledge of basic ionization processes and for laser technology and industry. The peculiar characteristics of femtosecond laser interaction are related to the dependence of the material modifications to the incident laser intensity, which can be extremely high ($\sim 10^{14}$ W/cm^2) while the deposited energy is kept moderate ($\sim \mu$J). Femtosecond laser interaction involves several complex phases and phenomena occurring on different time scales from femtosecond to nanosecond.[1–7] In dielectric materials, contrary to metals, the conduction band is initially empty and the matter is transparent to the laser light. Electrons from the valence band must be first transferred in the conduction band by nonlinear ionization processes to start the laser heating. The initial generation of conduction electrons occurs by photo-ionization process which depends on the laser field and material.[8] When the photo-ionization process is initiated, the seed electrons excite into the conduction band then absorb the laser energy. If the kinetic energy of the conduction electrons exceeds a critical value, they can further ionize other bound electrons in the valence band inducing the avalanche ionization process. The ionized dielectric medium starts to behave like a metal with a time varying electron density in the conduction band. The deposited laser energy is then transferred to the lattice, and thermomechanical relaxation and ejection of matter processes occur depending on the amount of absorbed laser energy density.

To provide valuable information on the effective ionization mechanisms, and to progress toward accuracy and predictability of the material behavior exposed to femtosecond laser irradiation, the precise experimental knowledge and theoretical analysis of damage and ablation thresholds are essential. The problem of laser damage and ablation measurement in the femtosecond regime has already been addressed in the literature, with a variety of ex-situ investigations of the morphological changes incurred by the target,[9–17] and in-situ measurements tracking the properties of the created plasma or any change in the optical properties of the studied sample.[9,13,18–22] Nevertheless, they are often difficult to use and compare due to the variety of experimental setups and measurement procedures. In this study, we perform a simple experiment to precisely evaluate in the same operating conditions the behavior of the damage and ablation thresholds under the wide excursion of a single experimental interaction parameter, i.e., the pulse duration. The experiments, described in Sec. II, are performed in the single shot regime to avoid any incubation effects and on a well-known dielectric material (fused silica). After a description of the modeling incorporating the absorption of the laser energy in the material and its subsequent relaxation (Sec. III), we then confront our experimental set of data to the numerical results (Sec. IV), providing a good comparison of the ionization processes of a dielectric material irradiated by ultrashort (few cycle laser pulses) to sub-picosecond (300 fs) laser pulses at the level of damage and ablation thresholds.

II. EXPERIMENTS

Experiments are performed using a KMLabs laser source delivering linearly polarized 25 fs 5 kHz pulses at 800 nm. Self phase modulation (SPM) in a hollow-core fiber (HF) filled with argon generates a wide spectrum recompressed by chirped mirrors to reach bandwidth-limited 7 fs pulses.[23] 30 fs pulses are obtained by replacing argon with helium such that SPM is completely suppressed. 100 fs pulses are obtained by limiting the spectrum width in the compressor of the commercial 25 fs source, whereas 300 fs pulses are produced by introducing a controlled chirp with an acousto-optic filter before the HF. The HF also acts as a spatial filter, selecting only the fundamental mode. The combination of a half-wave plate and a pair of reflective Germanium plates at the Brewster angle enables

variable attenuation to finely control the pulse energy incident on the target sample. The linearly polarized beam is focused at normal incidence by an off-axis parabolic mirror of 50 mm focal length, leading to a focal spot of radius $w_0 = 4.65\ \mu$m $\pm 5\%$ at $1/e^2$ (measured by imaging on a CCD camera) with a nearly-Gaussian intensity distribution. The laser fluence F is expressed by $F = 2E/\pi w_0^2$, where E is the laser energy and w_0 is the beam waist, considering the local peak fluence. The targets are 2-mm-thick high-purity superpolished fused silica discs (a-SiO_2 Suprasil from Heraeus, bandgap: $E_g = 8.9$ eV) with impurity <0.065 ppm and residual roughness $Ra = 0.2$ nm measured by AFM. Precise positioning of the target surface at the focal plane is obtained by combined energy-scan and z-scan procedures. All the experiments are performed under ambient air in the single shot regime, ensured by fast translation of the sample (25 cm/s) in front of the 5 kHz laser beam. The interval between adjacent damages is 50 μm, which is five times larger than the largest damages, so that contamination by possible redeposition of debris in a neighbor impact is prevented.

Previously, we defined dedicated procedures and methodologies to accurately distinguish and determine the damage and ablation fluence thresholds using a single experiment.[24] The experiment simply consisted in the realization of single shot sequences comporting a large number of trials at different energy levels on the surface of a dielectric material. Afterwards, a statistical analysis of the damage occurrence leads to the precise determination of the energy level for which no damage is reported. Then, the corresponding damage threshold fluence can be determined taking into account the beam surface. In this study, the damage is classically defined[11] as the occurrence of any visible permanent alteration of the surface as seen with a high resolution optical microscope.This diagnostic is fully consistent with the AFM analysis showing a molten zone corresponding to the beam center [see Fig. 1(a)]. Using the same set of data and an accurate diagnostic tool able to measure a quantitative ablation parameter, like the diameter of a laser-induced crater or the ablated volume as done in this work [e.g., with an AFM, see Fig. 1(b)], one can further determine by regression the corresponding ablation threshold.[24]

Here, we apply the principle of such an experiment to precisely evaluate in the same operating conditions the damage and ablation thresholds of fused silica. Figure 2 depicts the evolution of the damage and ablation thresholds for pulse durations ranging from sub-10 fs to a few hundred (300 fs) femtosecond pulses. Both thresholds follow qualitatively the same evolution with a strong reduction of their values for pulse durations below 30 fs and a slow increase at longer pulse duration. The relative evolution of both thresholds as a function of pulse duration evidenced in Fig. 2 is in good accordance with results of the literature.[1,9,14,15,25,26] The methodology we applied provides additional information, yielding distinctive evolutions of the damage and ablation thresholds over a wide range of pulse durations, spanning from few optical cycle (7 fs) to the sub-picosecond (300 fs) regime. In addition, the experiment is done in the single-shot regime, thus avoiding the complexity of cumulative effects encountered in the single previous study[15] done in a similar pulse duration range.

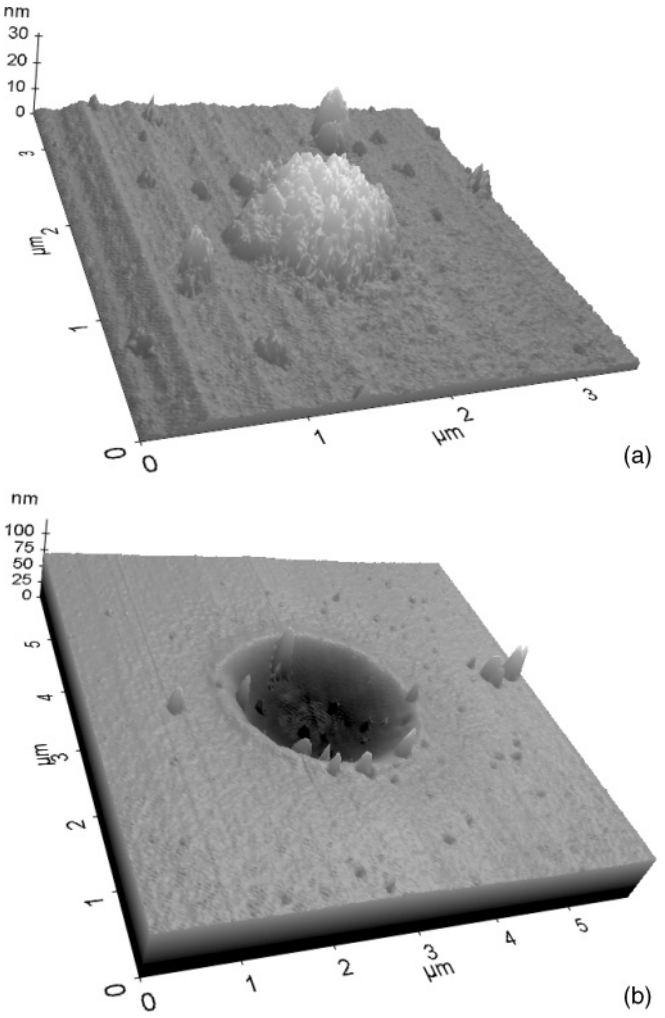

FIG. 1. AFM images of the material after irradiation by a single fs pulse at a fluence close to the damage (a) and ablation (b) threshold. The laser beam diameter is $2w_0 = 9.3\ \mu$m. The examples shown here are taken from the 30 fs experiment and correspond to $F = 2$ J/cm^2 (a) and $F = 2.7$ J/cm^2 (b). Similar results have been obtained at all experimental pulse durations.

III. MODEL

Dielectric materials are initially transparent to 800 nm laser pulses as their conduction band is empty. However, if the laser intensity is sufficiently high, transitions of electrons from the valence to the conduction band can occur through nonlinear absorption processes during the laser irradiation. Further, a part of the laser energy is absorbed by the ionized material leading to the heating of the lattice. Material ionization is therefore a fundamental process in femtosecond laser interactions with dielectric materials. Commonly, this process is described by a simple rate equation, combining the effects of the photoionization (PI) and of the impact (or, avalanche) ionization (II).[11] The total rate of electron generation is written as

$$\frac{\partial n_e}{\partial t} = \frac{n_v - n_e}{n_v}\left(w_{\mathrm{PI}} + n_e w_{\mathrm{II}}\right) - \frac{n_e}{\tau_r}, \qquad (1)$$

where n_e is the electron density in the conduction band, n_v is the initial electron density in the valence band, and w_{PI} and

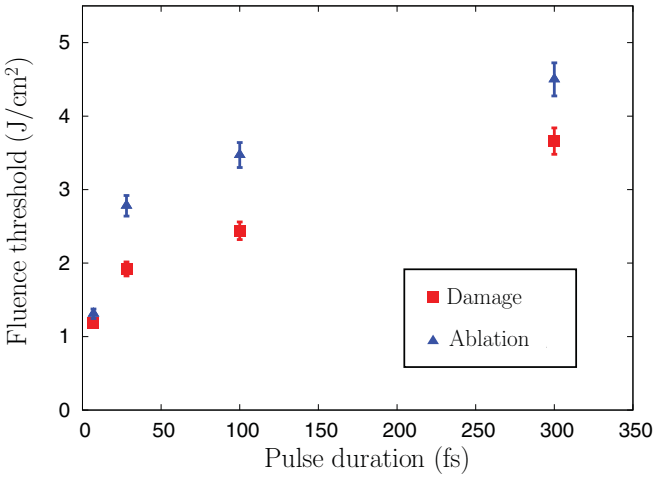

FIG. 2. (Color online) Damage and ablation fluence thresholds as a function of laser pulse duration. The error bars correspond to shot-to-shot energy fluctuations measured to be about 10% for all pulse durations.

w_{II}, respectively expressed in $cm^{-3}\,s^{-1}$ and s^{-1}, are the rates of photoionization and avalanche. The last term in Eq. (1) accounts for free electron decay, and τ_r is the corresponding time constant ($\tau_r = 150$ fs in fused silica[27]).

Two main recombination processes can occur depending on matter ionization.[28] At low electron density, the electron recombination takes place primarily by binary collisions with the emission of a photon. When the electron density increases, the electron recombination process evolves to three-body collisions with an electron acting as the third body. In this study, we assume that in each case the kinetic and potential energies, carried by a photon or an electron, are transferred to the conduction electrons. However, the free-carrier relaxation leads to the production of metastable self-trapped excitons (STE).[29,30] Indeed, these defects, mainly corresponding to E centers situated ~6 eV under the conduction band, are easily produced in amorphous fused silica[29,31] upon ionizing or laser irradiation, and yield to densification of the lattice. The dynamics of creation and extinction of these defects following laser excitation has been studied by several authors, estimating a trapping time in the range of 150 fs (τ_r) and complex relaxation pathways made of fast ($\gg$10 ps) and slow (ms) components.[27,29–31] Interestingly, recent experimental results[30] indicate that the relaxation to E centers constitutes the main energy relaxation pathway of the free-electron gas produced by laser excitation. As the electrons are trapped in an excited state over the valence band (~3 eV), the potential energy transferred to the conduction electrons is smaller than the band gap energy.

Moreover, when the pulse duration is greater than the recombination time, STE can be retransferred to the conduction band by PI or II. To include the formation of STE in our model, the rate of electron generation is given by

$$\frac{\partial n_e}{\partial t} = \frac{n_v - n_e}{n_v} w_g + \frac{n_s}{n_a} w_s - \frac{n_e}{\tau_r}, \tag{2}$$

$$\frac{\partial n_s}{\partial t} = \frac{n_e}{\tau_r} - \frac{n_s}{n_a} w_s, \tag{3}$$

where $w_g = w_{PI}(U_g) + n_e w_{II}(U_g)$, and $w_s = w_{PI}(U_s) + n_e w_{II}(U_s)$ ($U_g = 9$ eV is the band gap for valence electrons, and $U_s = 6$ eV is the STE band gap). n_s is the STE density, and n_a is the atom density.

The photoionization process depends directly on laser intensity.[8] The PI corresponds to the multiphoton absorption (MPI) in the low field limiting case of the Keldysh theory, and to the tunneling effect (TI) in the high field case. As in this work we consider a wide range of electric laser fields, where either tunneling or multiphoton effects can prevail depending on pulse duration, the photoionization rate w_{PI} is expressed by the Keldysh formulation for solids,[8]

$$w_{PI} = \frac{2\omega}{9\pi}\left(\frac{\omega m^*}{\hbar\gamma_1}\right)^{3/2} Q(\gamma,x) \times \exp\left[-\pi\,\langle x+1\rangle\,\frac{K(\gamma_1)-E(\gamma_1)}{E(\gamma_2)}\right], \tag{4}$$

where the symbol $\langle x\rangle$ denotes the integer part of the number x, and $\gamma = \omega\sqrt{m^* U}/eE_l$ is the Keldysh parameter for the band-gap U and applied laser electric field E_l. $m^* = m_e/2$ is the electron reduced mass, e the electron charge, and ω the laser pulsation. The functions K and E are the complete elliptic integrals of the first and second kind, $\gamma_1 = \gamma/\sqrt{1+\gamma^2}$ and $\gamma_2 = \gamma_1/\gamma$. The function $Q(\gamma,x)$ in Eq. (4) is :

$$Q(\gamma,x) = \sqrt{\frac{\pi}{2K(\gamma_2)}}\sum_{n=0}^{\infty}\exp\left[-\pi n\,\frac{K(\gamma_1)-E(\gamma_1)}{E(\gamma_2)}\right] \times \Phi\left[\pi\sqrt{\frac{2\langle x+1\rangle - 2x + n}{2K(\gamma_2)E(\gamma_2)}}\right], \tag{5}$$

where $\Phi(z) = \int_0^z \exp(y^2 - z^2)dy$, and $x = \tilde{U}/\hbar\omega$. $\tilde{U}$ is the effective bandgap, given by:

$$\tilde{U} = \frac{2U}{\pi\gamma_1}E(\gamma_2). \tag{6}$$

Figure 3 presents the evolution of photoionization rate estimated by Eq. (4) for $U = U_g$ with the laser intensity I_l,

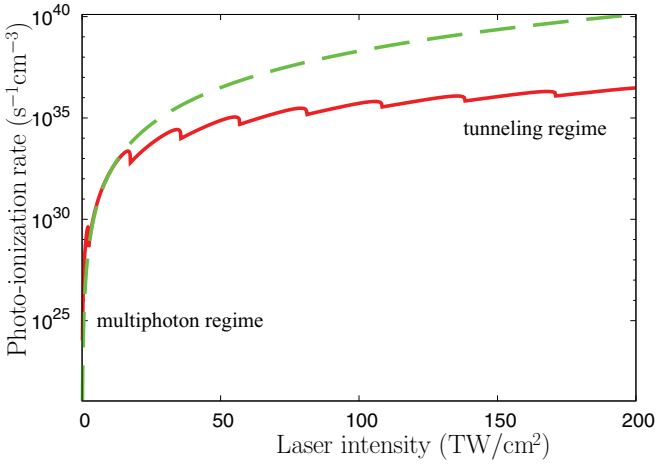

FIG. 3. (Color online) Photo–ionization rate as a function of laser intensity for $\lambda_l = 800$ nm in SiO_2 estimated by the Keldysh formulation (solid line) and the multiphoton approximation (dashed line).

$I_l = c\varepsilon_0|E_l|^2/2$. The usual multiphoton approximation $\sigma_N I_l^N$ is also presented. For $\lambda_l = 800$ nm, $N = 6$ and $\sigma_6 = 2 \times 10^{25}$ cm^{-3}s^{-1}(cm^2/TW)^6 for SiO_2.[32]

For low laser intensities, the photoionization estimated by Eq. (4) corresponds to the multiphoton approximation. TI is negligible, and the valence electrons are transferred into the conduction band by multiphoton absorption. As the effective band gap increases with the laser intensity in the Keldysh formulation [see Eq. (6)], the multiphoton absorption effect becomes less efficient and the photoionization rate becomes smaller than the rate estimated by the multiphoton approximation. At the same time, the probability of tunnel effect increases with the ponderomotive energy, i.e., laser field, and becomes higher than the probability of multiphoton ionization. At high intensity, the valence electrons are thus promoted in the conduction band by tunnel effect. In contrast to PI, the II process occurs when the kinetic energy of a free electron is high enough to overcome the ionization potential, and to transfer an electron from the valence band into the conduction band by collision.[33]

The impact ionization is generally assumed to depend on the laser electric field and on the electron number density in the conduction band.[11,14,15,34] However, this process requires electrons with high kinetic energy. The photoionization, on the contrary, generates electrons with low kinetic energy in the conduction band.[35] The energy of conduction band electrons increases by laser energy absorption (Joule heating), which can take time comparable with the laser pulse duration. A model of the impact ionization that describes the conduction band as a succession of discrete energy levels was recently proposed.[5,36] In this model, a conduction band electron successively absorbs a set of photons from the laser light leading to a gradual increase of its energy. When the energy of an electron in the conduction band is sufficiently high, the impact ionization can occur. Here we use a different model for the impact ionization process based on a reduced kinetic model and a Fermi distribution for describing the free electron subsystem.

The time required for electron-electron equilibrium is inversely proportional to the electron-electron collision rate and depends on the free electron density. The lifetime of an excited electron in a degenerate system is given by the Fermi-liquid theory under the random-phase approximation.[37] This time increases with the carrier density, and for an absorbed energy of 1.5 eV (energy of one photon in your conditions) and a carrier density of 2.2×10^{22} cm^{-3} (corresponding to single molecular ionization), the thermal equilibrium is obtained in a time less than 5 fs. For smaller electron density, this time reduces and thus the former duration of 5 fs can be considered as the maximum time for obtaining a complete Fermi distribution for the free electron population.

Although the problem of electron thermalization is rather complicated, this simple model gives us an order of the thermalization time value, and we assume that the electron distribution is always close to an equilibrium distribution even for 7 fs pulses. Then, as in Ref. 38, the electrons in the conduction band are described by the Fermi distribution instead of a set of discrete energetic levels used in Ref. 36. The advantage of this model is that it allows us not only to use a temperature-dependent ionization rate, but also to self-consistently describe the electron energy, enabling us to simply infer the time evolution of the material optical properties.

The impact ionization rate can be written as $w_{\mathrm{II}} = \int \nu_0(\varepsilon)F_e(\varepsilon)d\varepsilon$, where F_e is the electron energy distribution function and $\nu_0(\varepsilon) = \alpha_0(\varepsilon/\Delta - 1)^2$ for $\varepsilon > \Delta$, and zero for $\varepsilon < \Delta$.[33] The critical energy Δ corresponds to the minimum kinetic energy of the colliding free electron needed to fulfill energy and momentum conservation.[39] We take $\Delta = (3/2)\tilde{U}$, as we assume the effective mass of electron and hole are both equal to the free electron mass. The rate constant α_0 is 1.5 fs^{-1} for fused silica.[11] By assuming a Fermi distribution for the electrons in the conduction band, and a density of state $g(\varepsilon) = (1/2\pi^2)(2m_e/\hbar^2)^{3/2}\sqrt{\varepsilon}$, the electron energy distribution function is

$$F_e(\varepsilon) = \frac{3}{2}\left(\frac{\varepsilon}{E_F^3}\right)^{1/2} f_F(\varepsilon), \tag{7}$$

where $f_F(\varepsilon)$ is the Fermi distribution function, and E_F is the Fermi energy,

$$E_F = \frac{\hbar^2(3\pi^2 n_e)^{2/3}}{2m_e}. \tag{8}$$

The ionization process locally transforms the dielectric material into an absorbing plasma with metallic properties. The electrons in the conduction band are heated by the laser, and transfer their energy to the lattice. The ionized part of the dielectric can be described by the two-temperature model,[32,38] and the energy conservation law is[40]

$$C_e\frac{\partial T_e}{\partial t} = -\left.\frac{\partial S_l}{\partial z}\right|_{z=0} - \gamma_{\mathrm{ei}}(T_e - T_i) + W_I, \tag{9}$$

$$C_i\frac{\partial T_i}{\partial t} = \gamma_{\mathrm{ei}}(T_e - T_i), \tag{10}$$

where γ_{ei} is the electron-lattice coupling factor, and C_e and C_i are the electron and lattice heat capacity, respectively. The electron heat capacity is

$$C_e(T_e,n_e) = \rho\int_{-\infty}^{\infty}\frac{\partial f_F(\varepsilon)}{\partial T_e}\,g(\varepsilon)\,\varepsilon\,d\varepsilon, \tag{11}$$

and the lattice heat capacity[3] is $C_i = 1.6$ J/(cm^{3}K).

The last term in Eq. (9) corresponds to the potential energy transferred to the electrons during the recombination process, and the electron energy losses during the collisional ionization process,

$$W_I = \tilde{U}_s n_e\left[\frac{1}{\tau_r} - \frac{n_s}{n_a}\,w_{\mathrm{II}}(U_s)\right] - \frac{n_v - n_e}{n_v}\,\tilde{U}_g w_{\mathrm{II}}(U_g). \tag{12}$$

In Eq. (9), S_l is the absorbed energy flux

$$S_l = [1 - R(z=0,t)]\,I_l(t)\,\exp\left(-\frac{2z}{l_p}\right), \tag{13}$$

where $I_l(t)$ is the intensity of the incident laser pulse, R is the reflectivity at the surface, which is expressed by the Fresnel equations, and $l_p(z,t) = c/(\omega\kappa)$ is the skin depth of the material. κ is the complex part of the index of refraction.

We note here that the ionization of the matter is confined to a small layer at the surface during the temperature equilibration time for laser intensity near the damage and ablation thresholds.[3] Then, considering this temporal window,

the electronic heat conduction can be neglected in Eq. (9). Moreover, as we focus on the material surface, the laser energy losses by photoionization upon propagation in the absorbing material are not taken into account in Eq. (13). The optical properties of the matter are determined by using the complex dielectric function $\epsilon(z,t)$ given by

$$\epsilon = \epsilon_i - \frac{\omega_p^2}{\omega_l(\omega_l + i\nu_e)}, \tag{14}$$

where $\omega_p = \sqrt{n_e e^2/m_e\varepsilon_0}$ is the plasma frequency, ν_e is the effective electronic collision frequency, and ϵ_i is the dielectric constant of the unexcited material ($\epsilon_i = 2.25$ for SiO_2[20]).

The effective electronic collision frequency ν_e corresponds to the sum of the electron-phonon and electron-electron collision frequencies,[41] $\nu_e = \nu_{ep} + \nu_{ee}$, for low electronic temperature ($T_e < T_F$). At high electron temperature ($T_e \gg T_F$), ν_e is approximated by the electronic collision frequency in plasma, which is the sum of electron-neutral and electron-ion collision frequencies,[42] $\nu_e = \nu_{en} + \nu_{ei}$. In the temperature domain between these two limits, an upper cutoff ν_c is introduced by the requirement that the electron mean free path cannot be smaller than the ion sphere radius.[43] The effective electronic frequency ν_e is then expressed as the harmonic mean between these different components,

$$\nu_e^{-2} = (\nu_{ep} + \nu_{ee})^{-2} + (\nu_{en} + \nu_{ei})^{-2} + \nu_c^{-2}. \tag{15}$$

The electron-phonon and electron-electron collision frequencies are respectively[43] $\nu_{ep} \sim T_i/v_F$, where $v_F \sim n_e^{1/3}$ is the Fermi velocity, and[41] $\nu_{ee} \sim T_e^2/E_F$. Then, these collision frequencies are given by $\nu_{ep} = A_{ep}T_i/n_e^{1/3}$ and $\nu_{ee} = A_{ee}T_e^2/n_e^{2/3}$, where A_{ep} and A_{ee} are two constants. We have chosen $A_{ep} = 4 \times 10^{18}$ K^{-1} cm^{-1} s^{-1} and $A_{ee} = 8 \times 10^{18}$ K^{-2} cm^{-2} s^{-1} in our simulations for fused silica. This choice will be justified in Sec. IV. The collision frequencies in plasma are given by $\nu_{en} = 2 \times 10^{-7}(n_v - n_e)T_e^{1/2}$ and $\nu_{ei} = 2.91 \times 10^{-6} Z n_e \Lambda T_e^{-3/2}$, where Λ is the Coulomb logarithm.[44] The maximum collision frequency reads[43] $\nu_c = v_e V^{1/3}$, where v_e is the characteristic electron velocity, and $V = 4\pi n_a/3$.

The coupling factor γ_{ei} in Eqs. (9) and (10) is estimated by[45] $\gamma_{ei} \sim n_e \nu_{ep}(T_e)/T_e$, where $\nu_{ep}(T_e)$ is the electron-phonon collision frequency at the electron temperature T_e. Then, $\gamma_{ei} = \gamma_0 n_e^{2/3}$, where γ_0 is a material constant. $\gamma_0 = 0.6 \times 10^{-3}$ W/(Kcm) in our simulations.

IV. RESULTS AND DISCUSSION

The damage and ablation thresholds are often related to the electron density in the conduction band, and particularly to the critical electron density.[11,14,15,46] When the electron density exceeds the critical electron density ($n_c = 1.7 \times 10^{21}$ cm^{-3} in fused silica for a laser wavelength of 800 nm), the material turns highly absorbing. The criterion $n_e = n_c$ thus appears as a necessary condition for dramatic modification (ablation and/or damage) of a material, but in general does not describe with the highest accuracy the exact numerical and experimental conditions yielding such profound changes of the material. As a result, some authors[17,42,47] suggest using an energetic criterion related to experimental inspection of the material, that is a minimum energy density to be deposited within the material able to cause observable damage. For instance, this minimum energy density is taken as the energy density barrier under equilibrium conditions, including the energy to heat and to decompose the sample (for fused silica, $E_b = 54$ kJ/cm^3). In our model, we introduce two different criteria, also based on energetic considerations and experimental evidence, but in addition able to differentiate the damage and ablation thresholds and to account for the possible influence of strong nonequilibrium conditions.

Experimentally, a damage induced at the surface of the dielectric material by the laser pulse is typically related to any permanent change in the surface topology as evidenced by an optical microscope.[11,24] In our theoretical study, we interpret the damage as a material phase transition from solid to liquid phase. Numerically, the damage threshold then corresponds to the fluence for which the lattice temperature exceeds the melting temperature of the material T_m[38,48] (1800 K for fused silica). Note this interpretation is fully consistent with the experimental definition and the experimental observations performed very close to the damage threshold. Indeed, as shown in Fig. 1(a), the AFM analysis done very close to the damage threshold reveals a slightly elevated molten zone (few tens nm high) centered with respect to the beam but of much smaller radial extension and yielding to modifications of the surface topology but no significant material ablation.

Further increase of the laser fluence above the damage threshold fluence (at a given pulse duration) yields to high free electron energy that may overcome the ion binding energy. Atoms and molecules are then ejected from the target by electron-driven ablation process,[2,3,13,49] leaving a crater in the material as evidenced with the AFM analysis [see Fig. 1(b)]. As in Ref. 49, we thus define numerically the ablation threshold fluence as that yielding a surface electron temperature in excess of the cohesion temperature $T_{ec}(T_i,n_e)$. This temperature is defined as the electron temperature, for which the isotherm (T_e,T_i) passes by the nonequilibrium critical point where $\partial P/\partial\rho = \partial^2 P/\partial\rho^2 = 0$ (P is the pressure, and ρ is the lattice density). This criterion, by taking into account the energetic contributions of the electrons and ions and strong nonequilibrium conditions, then accounts more precisely for transient energetic processes occurring at short time scale and able to yield material ablation. Note that the occurrence of strong nonequilibrium conditions should also influence the process of damage. However, as there is no loss of material at any time, we argue that the total energy deposited in the material (first in the electron subsystem and further transmitted to the ions) is ultimately dissipated in the material keeping the same mass (no ablation), and yielding to macroscopic damage under equilibrium conditions (fusion). As a result, the chosen criterion for damage ($T_i = T_m$), well in accordance with our experimental observations, also correctly describes the occurring phenomena.

To calculate the cohesion temperature, the pressure in the heated matter is expressed as the sum of the electron and ion pressures. The electron pressure $P_e(T_e,n_e)$ is obtained from the Fermi model. The ion temperature is defined as $P_i(T_i,n_e) = P_{SES}(T_i,\rho_s) - P_e(T_i,n_e)$, where the electron pressure at the ion temperature $P_e(T_i,n_e)$ is subtracted from the total pressure at the ion temperature provided by the SESAME table 7387 $P_{SES}(T_i,\rho_s)$, with ρ_s the solid density.[50]

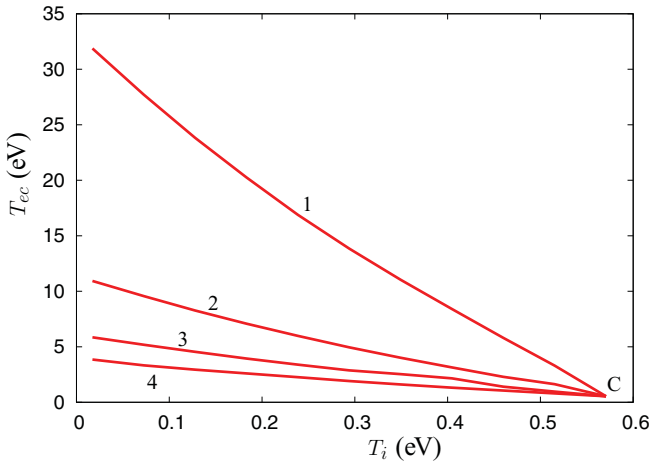

FIG. 4. (Color online) Evolution of the cohesion temperature T_{ec} with the ion temperature T_i for $n_e = 2.2 \times 10^{21}$ (1), 6.6×10^{21} (2), 1.3×10^{22} (3), and 2.2×10^{22} cm^{-3} (4). The point C is the classical critical temperature.

Figure 4 presents the cohesion temperature T_{ec} as a function of the lattice temperature T_i for different electron densities in the conduction band. As the ion temperature increases, the cohesion temperature decreases for all electron density and tends to the classical critical temperature (point C in Fig. 4). Moreover, for the same lattice temperature value, T_{ec} decreases as the electron density increases in the conduction band. Then, our definition of the cohesion temperature takes into account the ionization and lattice heating effects in the ablation process of matter.

The model presented in Sec. III is now applied to determine the damage and ablation thresholds of fused silica for pulse durations between 7 and 350 fs. The two criteria introduced above, $T_i = T_m$ for the damage threshold and $T_e = T_{ec}(T_i, n_e)$ for the ablation threshold, are used to evaluate the two thresholds. Figure 5 then groups the evolution of both

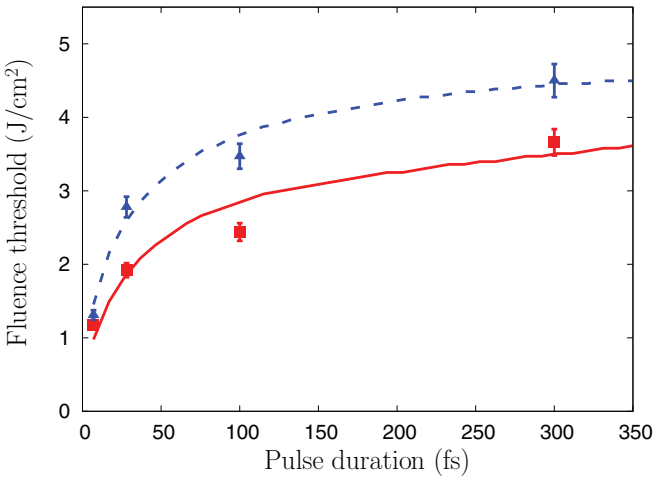

FIG. 5. (Color online) Evolution of the damage and ablation fluence thresholds as a function of laser pulse duration: experimental data (squares and triangles corresponding respectively to damage and ablation) compared to numerical simulations (solid and dashed lines corresponding respectively to damage and ablation).

calculated damage and ablation thresholds together with the experimental data. The best agreement between theory and experiments is obtained for the following choice of material parameters.

Firstly, the coupling factor γ_{ei} is approximated by $\gamma_{ei} = \gamma_0 n_e^{2/3}$, with the material constant γ_0 set to $\gamma_0 = 0.6 \times 10^{-3}$ W/(Kcm). Note that an increase (resp. decrease) of the constant γ_0 yields a global decrease (resp. increase) of both damage and ablation thresholds for the whole range of pulse durations. In fact, together with the evolution of the electron density, the parameter γ_0 sets the rate of energy transfer to the lattice. For higher γ_0, the ion heating is more efficient and the cohesion temperature decreases. With our choice of γ_0, the temperature equilibration time is $\tau_{ei} = C_i/\gamma_{ei} = 3.3$ ps for $n_e = 2.2 \times 10^{22}$ cm^{-3}, which is within the typical range of electron-ion coupling time (between 1 and 30 ps).

Secondly, the two constants A_{ep} and A_{ee} fixing the magnitude of the electron-phonon and electron-electron collision frequencies (together with the evolution of the electron density) have been chosen to be consistent with the range of the electronic collision time values determined theoretically for fused silica:[51,52] $\nu_e = 10^{14} - 10^{16}$ s^{-1}. Slightly smaller values of the two constants A_{ep} and A_{ee} would yield an increase of the surface reflectivity and a lesser efficiency of the ionization processes and electron Joule heating, resulting in an increase of the damage and ablation thresholds, not in accordance with the experimental results.

Note that the three free parameters of the model, γ_0, A_{ep}, and A_{ee}, are determined considering physical arguments and independent measurements. Their correctness yields a good agreement between numerical and experimental threshold curves for the whole range of pulse duration (see Fig. 5). Considering Fig. 5, a decrease of both damage and ablation thresholds is observed as the pulse duration becomes shorter. Interestingly, a more abrupt decrease is observed for pulses $<$50 fs, and the two thresholds tend to merge at very short pulse durations ($\ll$50 fs).

We note also that the photoionization process of STE is negligible for the time pulse range considered (7–350 fs). The STE density is formed with a characteristic time of 150 fs and thus becomes significant at the end of the long laser pulses considered here, when the kinetic energy of electrons in the conduction band is sufficient to induce the impact ionization. Moreover, as the energy is conserved between the impact ionization of STE and the recombination processes, the STE ionization has no effect on the calculated damage threshold. But the STE ionization increases the ablation threshold for pulse durations greater than 50 fs as a part of the conduction electron energy used for STE impact ionization, thus lowering the maximum electron temperature in the conduction band.

The evolution of the electron density in the conduction band is a fundamental parameter of the laser-dielectric interaction. In the model presented in Sec. III, three different processes are considered: multiphoton absorption (MPI), tunnel effect (TI), and impact ionization (II). To determine the importance of each ionization process depending on the incident pulse duration, Eq. (2) is modified to neglect one or several ionization processes. Figure 5 presents the evolution of the damage threshold as a function of time pulse duration for different forms of Eq. (2): ionization estimated (i) by the

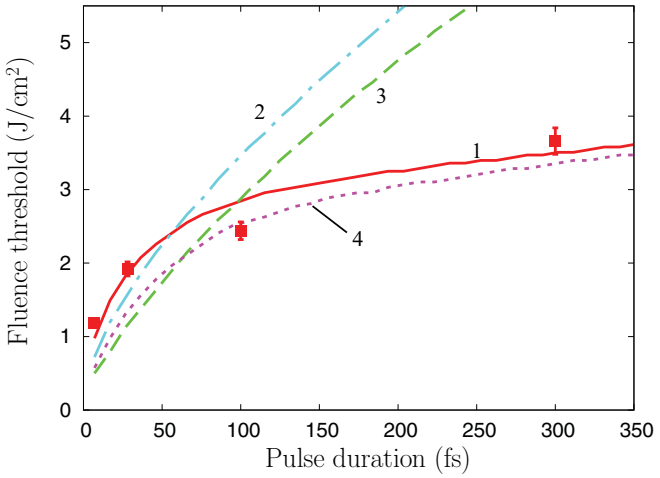

FIG. 6. (Color online) Damage fluence threshold evolution with the laser pulse duration for ionization rate estimated by the Keldysh formulation with avalanche process (1), by the Keldysh formulation only (2), by the multiphoton approximation (3), and by the multiphoton approximation with avalanche process (4). The squares present the experimental results corresponding to damage thresholds.

Keldysh formulation, which includes multiphoton absorption and tunnel effect, and with impact ionization process (curve 1), (ii) by the Keldysh formulation only (curve 2), (iii) by the multiphoton absorption approximation $\sigma_6 I_l^6$ (curve 3), (iv) by the multiphoton absorption approximation and impact ionization process (curve 4). The experimental results for the damage threshold are also presented.

The best agreement between the numerical results and the experimental data on the whole range of pulse durations is obtained for models including the impact ionization process (curves 1 and 4). The two models without II process, with only the MPI process [curve (3) in Fig. 6] or with only the Keldysh formulation [curve (2)], predict damage thresholds smaller than the experimental data for $\tau_l < 50$ fs, and greater for $\tau_l > 50$ fs. However, at short pulse durations, the estimated damage threshold is higher with the Keldysh formulation than with the multiphoton approximation. For pulse durations longer than 350 fs (not shown in Fig. 6), the threshold estimations of the two models are similar. When the pulse duration decreases, the laser intensity must be high to yield a photoionization rate important enough to create a sufficient number of seed electrons in the conduction band during the laser pulse. In that regime, the multiphoton absorption approximation largely overestimates the free electron generation rate compared to the case of the Keldysh formulation, which considers the progressive importance of tunnel ionization in the photoionization rate with the laser intensity increase (see Fig. 3). Comparing the results obtained with the avalanche ionization process along with the multiphoton approximation [curve (4) in Fig. 6] or the Keldysh formulation [curve (1)], we again note that the Keldysh formulation is necessary to correctly describe the damage thresholds at short pulse durations.

Two main conclusions can then be deduced here: (i) the photoionization cannot only be described by the multiphoton approximation at short pulse durations (<350 fs). This is related to the progressive significance of the tunnel ionization process as soon as the pulse duration is strongly reduced; (ii) the impact ionization process is predominant at long pulse durations ($\tau_l > 50$ fs) as underlined by several authors[5,36] but, importantly and according to our results, participates in matter ionization whatever the pulse duration. However, at very short pulse durations (<10 fs), its contribution is considerably smaller than photoionization.

Now, we propose an explanation of the evolution of the damage threshold on the whole range of pulse duration studied here. In particular, one should note that the damage threshold is increased by only a factor 3 between 7 and 300 fs while the ratio of pulse duration exceeds a factor 40. For a short laser pulse (<50 fs), the free electron generation rate issued from both photoionization (main absorption process) and II processes is fast, rapidly leading to a high free electron density and therefore a quick increase of the surface reflectivity and electron heat capacity.[41] In addition, the available time for consequent heating of the electron population by the laser is small (short pulse duration). As a consequence, a high intensity (correspondingly, relatively high fluence) is thus required for melting the material. For long pulse (>50 fs), the free electron density initially created through photoionization (mainly MPI) and further increased by II process is lower. The free electron population is easier to heat (slower increase of the surface reflectivity and electron heat capacity), and the time available for Joule heating and electron multiplication through II process is larger (long pulse). A moderate fluence (low intensity) is thus necessary for damaging the material.

Figure 7 presents the evolutions of the conduction electron density (a) and electron temperature (b) as a function of the normalized time $\bar{\tau} = (t - 3\tau_l)/\tau_l$ for the damage and ablation threshold fluences for $\tau_l = 7$ and 300 fs. The numerical damage and ablation threshold fluences are respectively $F = 1$ and 1.4 J/cm^2 for $\tau_l = 7$ fs, and $F = 3.5$ and 4.5 J/cm^2 for $\tau_l =$ 300 fs. The electron density n_e is normalized by the critical density $n_{cr} = 1.7 \times 10^{21}$ cm^{-3}, and the electron temperature T_e is normalized by the cohesion temperature $T_{ec}(T_i, n_e)$. The temporal shape of the pulse is presented in each figure.

Figure 7(a) shows that the maximum electron density is larger at the damage threshold for the short duration pulse than for $\tau_l = 300$ fs. This results from the high intensity required for melting at short pulse durations due to the very short time available for electron heating. In addition, the absence of electron-ion relaxation process (lattice heating) during the energy deposition due to the very short pulse duration ($\tau_l \ll \tau_{ei}$) favors the support of high free electron density. For longer pulses, the electron heating is more efficient and a smaller electron density is sufficient to yield a damage. At the ablation threshold, the electron density for the long pulse is closer to the electron density for $\tau_l = 7$ fs, and much higher than for the damage threshold. This is consistent with Fig. 4. Indeed, as the cohesion temperature decreases faster with the electron density than with the ion temperature, the electron density must be much more important than at the damage threshold for $\tau_l = 300$ fs.

Figure 7(b) shows that for the damage threshold fluences, the maximum electron temperature is $T_e = 0.2T_{ec}$, for $\tau_l =$ 300 fs. For $\tau_l = 7$ fs, the electron density is higher at the damage threshold, and the maximum electron temperature is $T_e = 0.5T_{ec}$. As a result, at very short pulse durations and in

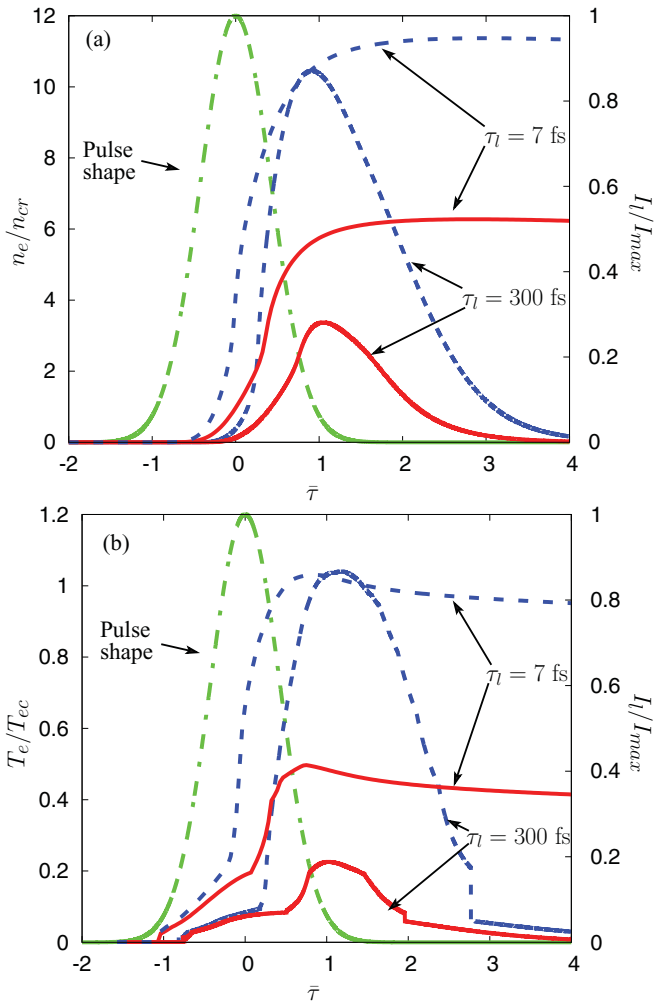

FIG. 7. (Color online) Evolutions of the conduction electron density (a) and electron temperature (b) as a function of the normalized time $\bar{\tau}$ for the damage (solid lines) and ablation (dashed lines) threshold fluences for $\tau_l = 7$ and 300 fs. The temporal pulse shape is also presented and corresponds to the right hand axis.

comparison with long pulses, the energetic difference (in terms of energy deposition) is small between the two thresholds (damage and ablation thresholds), which tend to coincide. In case of ablation at very short pulse durations and due to the very high free electron density, the rupture of cohesion of the material appears to be reached under thermodynamical conditions characterized by a rather low electronic and lattice (ionic) temperature. The time of matter ejection following the necessary condition $T_e = T_{ec}$ depends on the inertia of the ion population in response to the huge electronic field related to the creation of the high free electron density, which has been numerically evaluated to ~80 fs for Coulomb ablation.[53] Proper experimental and numerical evaluation of this time is out of the scope of this paper but should be addressed in the future. However, it is expected that this time is rather short ($\ll \tau_{ei}$), not allowing a significant rise of the lattice temperature before ejection of matter takes place. The ablation process when using very short pulse duration thus tends to be largely nonthermal (almost pure electronic ablation with minimum thermal effects) as evidenced in numerous other

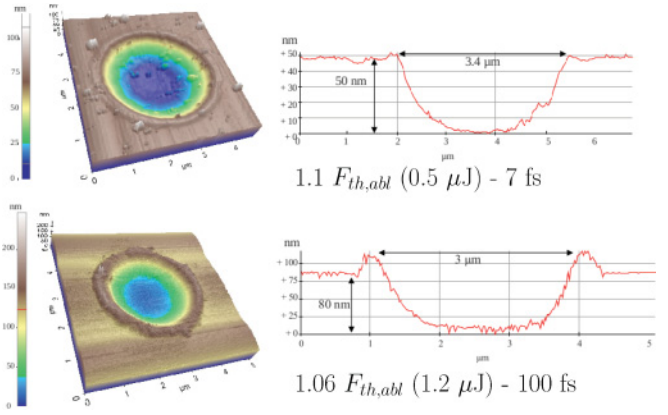

FIG. 8. (Color online) AFM 3D snapshot and 1D profile for two pulse durations (7 and 100 fs) and close to the ablation threshold ($F \approx 1.1\ F_{\text{th,ablation}}$ for 7 fs and $F \approx 1.06\ F_{\text{th,ablation}}$ for 100 fs). A thicker and higher elevated rim attributed to melting (Ref. 54) is evident at 100 fs pulse duration while it is negligible for 7 fs.

works.[3,13,49] For long pulses, it is easier to differentiate the two thresholds. At the damage threshold, the maximum free electron density remains sufficiently low to not drastically reduce the cohesion temperature T_{ec}. However, at the ablation threshold, the electron density is rather high (comparable to the electron density reached with short pulses) thus requiring large fluence as the ionization rate is lower, which explains the important difference between the damage and ablation thresholds at long pulse durations.

These last results confirm the primary importance of ultrashort pulses for surface micromachining applications, as evidenced in previous experiments.[55] Indeed, as damage and ablation thresholds are very close at very short pulse durations, it thus appears possible to machine a dielectric material with a very high quality of process (no side effects). This is clearly demonstrated in Fig. 8 comparing the quality of an ablated crater at 7 and 100 fs and showing no marks of significant melting, in particular at the beam edges, at very short pulse durations.

Note also that, in any case in Fig. 7(a), the free electron density exceeds the critical electron density n_{cr} underlining that this parameter is most probably not a satisfactory criterion for a precise evaluation of the damage threshold of a dielectric material.

V. CONCLUSION

In summary, we have considered damage and ablation of dielectric targets by femtosecond pulses. In particular, ionization mechanisms have been analyzed. For that purpose, we carefully measured in the same operating conditions the behavior of the damage and ablation thresholds with a single experimental varying parameter, i.e., the pulse duration (<10–300 fs). We also realized a comprehensive theoretical analysis taking into account the absorption of the laser energy and its relaxation in the material. The criteria to numerically assess the damage and ablation thresholds have been chosen consistently with experimental observations of the laser irradiated zone. They are respectively related to the lattice melting temperature T_m and the electronic cohesion temperature T_{ec}.

A comparison between the experimental and numerical results then yields several important conclusions for the understanding of basic ionization mechanisms of solid matter at moderate intensity (10^{13}–10^{14} W/cm^2) and ablation processes. Firstly, the photoionization cannot only be described by the multiphoton approximation at short pulse durations (<350 fs). This is related to the progressive significance of the tunnel ionization process as soon as the pulse duration is strongly reduced. Secondly, the impact ionization process participates to matter ionization whatever the pulse duration, its importance being predominant at pulse duration >50 fs. Finally, a good agreement between the experimental and theoretical results on the whole range of pulse durations is only obtained when both avalanche ionization process and photoionization approximated by the Keldysh formulation are taken into account.

Concerning the ablation processes, we put in evidence that the damage and ablation thresholds tend to coincide at very short pulse duration (<10 fs). This fact is related to the high value of the free electron density generated with short pulses, strongly reducing the electronic cohesion temperature T_{ec}. In these conditions, the results indicate that the ablation process is a pure electron-driven ablation and appears to be free of thermal effects.

ACKNOWLEDGMENTS

B.C., O.U., N.S., M.S., and T.I. thank the French ANR agency for financial support through the Festic-ANR-06-BLAN-0298-02 and Nanomorphing-ANR-07-BLAN-0301-03 projects. We are grateful to V. T. Tikhonchuk, L. Hallo and A. Bourgeade for discussions.

*chimier@lp3.univ-mrs.fr

[1] M. D. Perry, B. C. Stuart, P. S. Banks, M. D. Feit, V. Yanovsky, and A. M. Rubenchik, J. Appl. Phys. **85**, 6803 (1999).
[2] S. Sundaram and E. Mazur, Nat. Mater. **1**, 217 (2002).
[3] E. G. Gamaly, A. V. Rode, B. Luther-Davies, and V. T. Tikhonchuk, Phys. Plasmas **9**, 949 (2002).
[4] B. N. Chichkov, C. Momma, S. Nolte, F. von Alvensleben, and A. Tünnermann, Appl. Phys. A **63**, 109 (1996).
[5] A. Kaiser, B. Rethfeld, M. Vicanek, and G. Simon, Phys. Rev. B **61**, 11437 (2000).
[6] L. Hallo, A. Bourgeade, V. T. Tikhonchuk, C. Mezel, and J. Breil, Phys. Rev. B **76**, 024101 (2007).
[7] N. M. Bulgakova, R. Stoian, A. Rosenfeld, I. V. Hertel, and E. E. B. Campbell, Phys. Rev. B **69**, 054102 (2004).
[8] L. V. Keldysh, Sov. Phys. JETP **20**, 1307 (1965).
[9] H. Varel, D. Ashkenasi, A. Rosenfeld, R. Herrmann, F. Noack, and E. Campbell, Appl. Phys. A **62**, 293 (1996).
[10] A. Rosenfeld, M. Lorenz, R. Stoian, and D. Ashkenasi, Appl. Phys. A **69**, S373 (1996).
[11] B. C. Stuart, M. D. Feit, S. Herman, A. M. Rubenchik, B. W. Shore, and M. D. Perry, Phys. Rev. B **53**, 1749 (1996).
[12] O. Utéza, B. Bussière, F. Canova, J. P. Chambaret, P. Delaporte, T. Itina, and M. Sentis, Appl. Surf. Sci. **254**, 799 (2007).
[13] R. Stoian, A. Rosenfeld, D. Ashkenasi, I. V. Hertel, N. M. Bulgakova, and E. E. B. Campbell, Phys. Rev. Lett. **88**, 097603 (2002).
[14] A. C. Tien, S. Backus, H. Kapteyn, M. Murnane, and G. Mourou, Phys. Rev. Lett. **82**, 3883 (1999).
[15] M. Lenzner, J. Krüger, S. Sartania, Z. Cheng, C. Spielmann, G. Mourou, W. Kautek, and F. Krausz, Phys. Rev. Lett. **80**, 4076 (1998).
[16] A. Ben-Yakar and R. L. Byer, J. Appl. Phys. **96**, 5316 (2004).
[17] Q. Jia, Z. Z. Xu, X. X. Li, R. X. Li, B. Shuai, and F. L. Zhao, Appl. Phys. Lett. **82**, 4382 (2003).
[18] J. Siegel, D. Puerto, W. Gawelda, G. Bachelier, J. Solis, L. Ehrentraut, and J. Bonse, Appl. Phys. Lett. **91**, 082902 (2007).
[19] F. Quéré, S. Guizard, P. Martin, G. Petite, O. Gobert, P. Meynadier, and M. Perdrix, Appl. Phys. B **68**, 459 (1999).
[20] A. Q. Wu, I. H. Chowdhury, and X. Xu, Phys. Rev. B **72**, 085128 (2005).
[21] D. Du, X. Liu, G. Korn, J. Squier, and G. Mourou, Appl. Phys. Lett. **64**, 3071 (1994).
[22] M. Li, S. Menon, J. P. Nibarger, and G. N. Gibson, Phys. Rev. Lett. **82**, 2394 (1999).
[23] M. Nisoli, S. D. Silvestri, and O. Svelto, Appl. Phys. Lett. **68**, 2793 (1996).
[24] N. Sanner, O. Utéza, B. Bussiere, G. Coustillier, A. Leray, T. Itina, and M. Sentis, Appl. Phys. A **94**, 889 (2009).
[25] D. Giguère, G. Olivié, F. Vidal, S. Toetsch, G. Girard, T. Ozaki, and J.-C. Kieffer, J. Opt. Soc. Am. A **24**, 1562 (2007).
[26] L. Hoffart, P. Lassonde, F. Légaré, F. Vidal, N. Sanner, O. Utéza, M. Sentis, J.-C. Kieffer, and I. Brunette, Opt. Express **19**, 230 (2011).
[27] P. Audebert, P. Daguzan, A. DosSantos, J. C. Gauthier, J. P. Geindre, S. Guizard, G. Hamoniaux, K. Krastev, P. Martin, G. Petite, and A. Antonetti, Phys. Rev. Lett. **73**, 1990 (1994).
[28] Y. B. Zel'dovich and Y. P. Raizer, *Physics of Shock Waves and High-Temperature Hydrodynamic Phenomena* (Dover, Mineola, NY, 2002).
[29] K. Song and R. Williams, *Self-Trapped Excitons* (Springer-Verlag, Berlin, 1993).
[30] D. Grojo, M. Gertsvolf, S. Lei, T. Barillot, D. M. Rayner, and P. B. Corkum, Phys. Rev. B **81**, 212301 (2010).
[31] K. Tanimura, T. Tanaka, and N. Itoh, Phys. Rev. Lett. **51**, 423 (1983).
[32] C. Mézel, L. Hallo, A. Bourgeade, D. Hébert, V. T. Tikhonchuk, B. Chimier, B. Nkonga, G. Schurtz, and G. Travaillé, Phys. Plasmas **15**, 093504 (2008).
[33] L. V. Keldysh, Sov. Phys. JETP **11**, 369 (1960).
[34] P. P. Rajeev, M. Gertsvolf, P. B. Corkum, and D. M. Rayner, Phys. Rev. Lett. **102**, 083001 (2009).
[35] N. Burnett and P. Corkum, J. Opt. Soc. Am. B **6**, 1195 (1989).
[36] B. Rethfeld, Phys. Rev. Lett. **92**, 187401 (2004).
[37] W. S. Fann, R. Storz, H. W. K. Tom, and J. Bokor, Phys. Rev. B **46**, 13592 (1992).
[38] L. Jiang and H.-L. Tsai, J. Appl. Phys. **104**, 093101 (2008).
[39] B. Ridley, *Quantum Processes in Semiconductors* (Clarendon, Oxford, 1993).
[40] S. I. Anisimov, B. L. Kapeliovich, and T. L. Perel'man, Sov. Phys. JETP **39**, 375 (1974).

[41]N. W. Ashcroft and N. D. Mermin, *Solid State Physics* (Holt-Saunder, New York, 1976).
[42]J. R. P. Peñano, P. Sprangle, B. Hafizi, W. Manheimer, and A. Zigler, Phys. Rev. E **72**, 036412 (2005).
[43]K. Eidmann, J. Meyer-ter-Vehn, T. Schlegel, and S. Huller, Phys. Rev. E **62**, 1202 (2000).
[44]*NRL Plasma Formulary*, edited by J. D. Huba (Naval Research Laboratory Publication, Washington, DC, 2005).
[45]M. I. Kaganov, I. M. Lifshitz, and L. V. Tanatarov, Sov. Phys. JETP **4**, 173 (1957).
[46]B. C. Stuart, M. D. Feit, A. M. Rubenchik, B. W. Shore, and M. D. Perry, Phys. Rev. Lett. **74**, 2248 (1995).
[47]T. Q. Jia, Z. Z. Xu, R. X. Li, D. H. Feng, X. X. Li, C. F. Cheng, H. Y. Sun, N. S. Xu, and H. Z. Wang, J. Appl. Phys. **95**, 5166 (2004).
[48]F. Korte, S. Adams, A. Egbert, C. Fallnich, A. Ostendorf, S. Nolte, M. Will, J.-P. Ruske, B. N. Chichkov, and A. Tünnermann, Opt. Express **7**, 41 (2000).
[49]B. Chimier, V. T. Tikhonchuk, and L. Hallo, Phys. Rev. B **75**, 195124 (2007).
[50]Report on the Los Alamos Equation-of-State Library, *SESAME* (1983).
[51]D. Arnold, E. Cartier, and D. J. DiMaria, Phys. Rev. B **45**, 1477 (1992).
[52]D. Arnold and E. Cartier, Phys. Rev. B **46**, 15102 (1992).
[53]H.-P. Cheng and J. D. Gillaspy, Phys. Rev. B **55**, 2628 (1997).
[54]A. Ben-Yakar, A. Harkin, J. Ashmore, R. L. Byer, and H. A. Stone, J. Phys. D: Appl. Phys. **40**, 1447 (2007).
[55]M. Lenzner, J. Krüger, W. Kautek, and F. Krausz, Appl. Phys. A **68**, 369 (1999).